



Arctic autumn warming since 2002 dominated by changes in moisture modulated by multiple large-scale atmospheric circulations

Kailun Gao^a, Anmin Duan^{b,*}, Deliang Chen^d, Ji Wang^a, Bin Tang^{b,c}

^a Beijing Municipal Climate Center, Beijing 100089, China

^b State Key Laboratory of Numerical Modeling for Atmospheric Sciences and Geophysical Fluid Dynamics, Institute of Atmospheric Physics, Chinese Academy of Sciences, Beijing 100029, China

^c University of Chinese Academy of Sciences, Beijing 100049, China

^d Regional Climate Group, Department of Earth Sciences, University of Gothenburg, Sweden

ARTICLE INFO

Keywords:

Arctic
Autumn warming
Water vapor
Atmospheric circulations

ABSTRACT

The clear-sky downward longwave radiation related to water vapor (LW-WV) has been confirmed to be the dominant factor promoting the autumn warming in the Arctic in the boreal autumn. In this study, we reveal the spatiotemporal characteristics of the 2 m air temperature (t_2m), clear-sky downward longwave radiation (CDLW), and water vapor in the Arctic and the mechanism affecting the change in the autumn LW-WV. Since 2002, not only have the temporal variations in regional t_2m , CDLW, and water vapor been synchronous at the interdecadal scale, but their largest spatial variations have also mainly been located in the Barents-Kara Sea and the Chukchi Sea. A diagnosis of the atmospheric moisture budget shows that the change in the water vapor divergence is dominated by the change in the mean circulation dynamics in the Barents-Kara Sea, while the change in the thermodynamics caused by the changes in the local specific humidity and the mean circulation dynamics are both important to the change in the water vapor divergence in the Chukchi Sea. The positive phase in the Arctic Oscillation (AO) and the Pacific/North American Pattern (PNA) have contributed to the increase in the water vapor in the Barents-Kara Sea, while the positive phase in the North Atlantic Oscillation (NAO) and the PNA are responsible for the increase in the water vapor in the Chukchi Sea. Therefore, synergetic effects of the multiple large-scale circulations play an important role in the recent warming in the Arctic in autumn.

1. Introduction

Under the current global warming setting, the warming rate in the past decades is much higher in the Arctic than the global average, which is known as the Arctic amplification phenomenon (Serreze et al., 2000; Serreze and Francis, 2006; Screen and Simmonds, 2010; Coumou et al., 2018; Dai et al., 2019), and the amplification will continue in the future (Cai et al., 2021). However, as a region sensitive to climate change, the reasons for the warming in the Arctic are still controversial (e.g., You et al., 2021). The possible reasons mainly include surface albedo feedback (Screen and Simmonds, 2010; Taylor et al., 2013), temperature lapse rate feedback (Goosse et al., 2018; Stuecker et al., 2018), Planck feedback (Bony et al., 2006; Crook et al., 2011), atmospheric water vapor feedback (Graversen and Wang, 2009; Gordon et al., 2013; Taylor et al., 2013), cloud radiative forcing (Shupe and Intrieri, 2004; Middlemas et al., 2020), and atmospheric and ocean heat transport

(Graversen and Burtu, 2016; Beer et al., 2020). And vegetation-atmosphere-sea ice interactions could also have played a role (Jeong et al., 2014).

The warming rate in the Arctic varies in the different seasons. It is strongest in the autumn and winter and weakest in the summer (Screen and Simmonds, 2010). However, the effect of the sea-ice albedo feedback is weak or even absent in the cold season because of the absence of solar radiation, so the sea-ice albedo feedback has a limited effect on Arctic warming in the cold season. Previdi et al. (2020) emphasized the importance of atmospheric processes to the Arctic amplification. In many atmospheric processes, atmospheric water vapor, as an important greenhouse gas, plays an important role in influencing the Arctic amplification (Gordon et al., 2013; Pithan and Mauritsen, 2014). In recent decades, the peak value of the growth rate of the atmospheric water vapor has shifted to autumn in the Arctic, which is mainly related to the accelerated increase in the water vapor in the Barents-Kara Sea

* Corresponding author.

E-mail address: amduan@lasg.iap.ac.cn (A. Duan).

<https://doi.org/10.1016/j.atmosres.2021.105879>

Received 5 July 2021; Received in revised form 6 October 2021; Accepted 6 October 2021

Available online 11 October 2021

0169-8095/© 2021 The Authors.

Published by Elsevier B.V. This is an open access article under the CC BY-NC-ND license

(<http://creativecommons.org/licenses/by-nc-nd/4.0/>).

during this season (Rinke et al., 2019). A positive feedback mechanism has been proposed for this process; that is, the accelerated melting of the sea ice in the autumn expands the ice-free sea area, which promotes evaporation in the ice-free region and leads to an increase in the atmospheric water vapor (Boisvert and Stroeve, 2015). In turn, the increase in the atmospheric water vapor further increases the downward long-wave radiation, resulting in more sea ice melting. This mechanism also illustrates the role of downward long-wave radiation, i.e., as a bridge, in the atmospheric processes affecting the sea ice changes. Furthermore, Ghatak and Miller (2013) found that the positive feedback of atmospheric water vapor is a nonlinear process, which helps us understand why the water vapor content is not the largest in the season with the greatest warming in the Arctic.

As is well known, atmospheric water vapor, clouds, and the atmospheric temperature are the main factors affecting the intensity of the downward long-wave radiation. Some studies have reported that compared with clouds and the atmospheric temperature, the positive feedback caused by atmospheric water vapor is the key factor causing the Arctic amplification (Curry et al., 1995; Ghatak and Miller, 2013; Middlemas et al., 2020). Based on diagnostic analysis of the surface energy balance equation, it has been determined that the clear-sky downward long-wave radiation caused by water vapor is the dominant factor affecting Arctic amplification in the autumn and winter (Gao

et al., 2019). As for the mechanism relating the atmospheric water vapor and/or downward long-wave radiation to Arctic warming in the winter, Hegyi and Taylor (2017) found that phases of the Arctic Oscillation (AO) and the Arctic Dipole (AD) can affect the changes in the downward long-wave radiation in the Arctic. When the AD/AO is in the negative (positive) phase, the downward long-wave radiation exhibits a positive (negative) anomaly. Gong et al. (2017a) argued that the increase in the downward long-wave radiation in the Arctic in the winter is mainly due to the increase in the water vapor flux related to the poleward propagation of the Rossby waves into the Arctic. Luo et al. (2017) pointed out that the combination of the positive phase of the North Atlantic Oscillation (NAO) and the Ural blocking is an optimal circulation pattern that significantly increases the Barents-Kara Sea water vapor, which plays a major role in the warming of the Barents-Kara Sea and sea ice reduction in winter. Wang et al. (2020) found that the mean atmospheric flow plays a leading role in increasing the atmospheric water vapor in the Barents-Kara Sea, which finally contributes to the significantly interdecadal warming in winter. Clark et al. (2021) further suggested that the winter warming in the Chukchi Sea is mainly due to temperature advection caused by changes in the atmospheric circulation, and a similar conclusion was drawn for the Barents Sea (Chen et al., 2013). Therefore, atmospheric circulations have been considered playing a key role in regulating the winter warming in the Arctic. However, few studies focused on the effect of atmospheric circulations on autumn warming in the Arctic. In this study, we will further explore whether the atmospheric circulations affect the autumn warming in the Arctic.

$$\rho_w \delta(P - E) \approx -\frac{1}{g} \left(\int_0^{p_s} \left(\overline{\delta \mathbf{u}} \cdot \nabla \overline{q_1} + \overline{\delta q} \nabla \cdot \overline{\mathbf{u}_1} + \overline{\mathbf{u}_1} \cdot \nabla \overline{\delta q} + \overline{q_1} \nabla \cdot \overline{\delta \mathbf{u}} \right) dp + \int_0^{p_s} \overline{(\mathbf{u}' q')} dp + \delta S \right) \quad (2)$$

et al., 2019). As for the mechanism relating the atmospheric water vapor and/or downward long-wave radiation to Arctic warming in the winter, Hegyi and Taylor (2017) found that phases of the Arctic Oscillation (AO) and the Arctic Dipole (AD) can affect the changes in the downward long-wave radiation in the Arctic. When the AD/AO is in the negative (positive) phase, the downward long-wave radiation exhibits a positive (negative) anomaly. Gong et al. (2017a) argued that the increase in the downward long-wave radiation in the Arctic in the winter is mainly due to the increase in the water vapor flux related to the poleward propagation of the Rossby waves into the Arctic. Luo et al. (2017) pointed out that the combination of the positive phase of the North Atlantic Oscillation (NAO) and the Ural blocking is an optimal circulation pattern that significantly increases the Barents-Kara Sea water vapor, which plays a major role in the warming of the Barents-Kara Sea and sea ice reduction in winter. Wang et al. (2020) found that the mean atmospheric flow plays a leading role in increasing the atmospheric water vapor in the Barents-Kara Sea, which finally contributes to the significantly interdecadal warming in winter. Clark et al. (2021) further suggested that the winter warming in the Chukchi Sea is mainly due to temperature advection caused by changes in the atmospheric circulation, and a similar conclusion was drawn for the Barents Sea (Chen et al., 2013). Therefore, atmospheric circulations have been considered playing a key role in regulating the winter warming in the Arctic. However, few studies focused on the effect of atmospheric circulations on autumn warming in the Arctic. In this study, we will further explore whether the atmospheric circulations affect the autumn warming in the Arctic.

2. Material and methods

2.1. Data

The monthly Japanese 55-year Reanalysis (JRA-55) dataset for 1980–2017 developed by the Japan Meteorological Agency (Ebata et al., 2011; Kobayashi et al., 2015), with a horizontal spacing of $1.25^\circ \times$

2.2. Methods

In order to assess the contributions of the different processes to the difference in the water vapor in the Arctic between two periods, we used the moisture budget equation (Seager et al., 2010). In this study, the changes in any variables (represented by a dot in Eq. 1) between 1980–2001 (period 1) and 2002–2017 (period 2) are represented as follows:

$$\delta(\bullet) = (\bullet)_2 - (\bullet)_1 \quad (1)$$

The moisture budget equation can be written as

P and E are the precipitation and evaporation, respectively. $\overline{(\bullet)}$ denotes the monthly mean, $(\bullet)'$ denotes a departure from the monthly mean, p_s is the surface pressure, q is the specific humidity, \mathbf{u} is the horizontal vector of the wind, ρ_w is the density of water, and S is the surface contributions (Trenberth and Guillemot, 1995). However, the surface contributions are normally a few times smaller than the other terms (Seager et al., 2007), so its contribution can be negligible. The vertically integrated moisture flux convergence (Q_{div}) is equivalent to the long-term mean of $P - E$ (Seager and Vecchi, 2010; Seager et al., 2010; Gao et al., 2014). Therefore, $\rho_w \delta(P - E)$ is the change in the vertically integrated moisture flux convergence between the two periods.

The change in the vertically integrated moisture flux convergence is also regarded as the contributions of the changes in the thermodynamics (δTH), mean circulation dynamics (δMCD), and transient eddy (δTE). Eq. (2) can also be written as

$$\delta Q_{div} \approx \delta TH + \delta MCD + \delta TE \quad (3)$$

$$\delta TH = -\frac{1}{g} \int_0^{p_s} \nabla \cdot \left(\overline{\mathbf{u}_1} [\overline{\delta q}] \right) dp \quad (4)$$

$$\delta MCD = -\frac{1}{g} \int_0^{p_s} \nabla \cdot \left([\overline{\delta \mathbf{u}}] \overline{q_1} \right) dp \quad (5)$$

$$\delta TE = -\frac{1}{g} \int_0^{p_s} \nabla \cdot \delta(\overline{\mathbf{u}' q'}) dp \quad (6)$$

To further investigate the characteristics of the changes in thermodynamics (δTH) and the mean circulation dynamics (δMCD), the changes in these two terms can be decomposed into the effects of the moisture advection (A) and moisture convergence (D). Eqs. (4) and (5) can be rewritten as

$$\delta TH = \delta TH_A + \delta TH_D, \text{ and } \delta MCD = \delta MCD_A + \delta MCD_D \quad (7)$$

$$\delta TH_A = -\frac{1}{g} \int_0^{p_s} \left(\bar{\mathbf{u}}_1 \cdot \nabla [\delta \bar{q}] \right) dp \quad (8)$$

$$\delta TH_D = -\frac{1}{g} \int_0^{p_s} \left([\delta \bar{q}] \nabla \cdot \bar{\mathbf{u}}_1 \right) dp \quad (9)$$

$$\delta MCD_A = -\frac{1}{g} \int_0^{p_s} \left([\delta \bar{\mathbf{u}}] \cdot \nabla \bar{q}_1 \right) dp \quad (10)$$

$$\delta MCD_D = -\frac{1}{g} \int_0^{p_s} \left(\bar{q}_1 \nabla \cdot [\delta \bar{\mathbf{u}}] \right) dp \quad (11)$$

To examine changes in water vapor over the Arctic, the vertically integrated moisture flux Q and the divergence of the moisture flux Q_{div} were calculated as follows:

$$Q = \frac{1}{g} \int_{p_s}^{p_1} q u dp, Q_{div} = \frac{1}{g} \int_{p_s}^{p_1} \nabla \cdot (qu) dp \quad (12)$$

Here, $p_1=100$ hPa; g is the acceleration due to gravity; and the other variables have the same meaning as above.

The Arctic Oscillation Index (AO index) and the North Atlantic Oscillation Index (NAO index) were calculated according to the method provided by the National Centre for Atmospheric Research (National Center for Atmospheric Research Staff (NCAR), 2021). The AO index is defined as the time series PC1 of the surface pressure EOF1 in the Northern Hemisphere (20–90°N, 180°W–180°E), and the definition of NAO index is similar to that for the AO index but the region of focus is in the North Atlantic (20–80°N, 90°W–40°E). For the Pacific/North American Pattern index (PNA index), we adopted the definition provided by Wallace and Gutzler (1981): PNA index = $0.25 \times [Z^*(20^\circ\text{N}, 160^\circ\text{W}) - Z^*(45^\circ\text{N}, 165^\circ\text{W}) + Z^*(55^\circ\text{N}, 115^\circ\text{W}) - Z^*(30^\circ\text{N}, 85^\circ\text{W})]$. Z^* represents the standardized geopotential height values at 500 hPa. All indexes above were calculated using the JRA-55 dataset in boreal autumn (September–October–November). In addition, the 9-year Lanczos low-pass filtering was used to obtain the interdecadal signals (Duchon, 1979). Standard empirical orthogonal

function (EOF) analysis (Weare and Newell, 1977; Weare and Nasstrom, 1982) was used to identify the main spatiotemporal patterns of the t2m and the precipitable water over the Arctic in boreal autumn, and the sliding t -test was also used to determine the interdecadal turning points.

3. Results

3.1. Spatiotemporal characteristics of the autumn water vapor, t2m, and CDLW in the Arctic

In recent decades, the Arctic amplification has been well documented (Coumou et al., 2018; Dai et al., 2019). As shown in Fig. 1a, the Arctic warming amplitude in 2 m temperature (t2m) exceeded three times compared with the global average in autumn (Fig. 1a). In order to remove the effects of global warming, the variability of global average in t2m (Fig. 1a, orange dashed curve) was removed, and the time series of t2m in the Arctic with no global warming (NGW) signal is shown (Fig. 1b, black dashed curve). Obviously, the variabilities in t2m with NGW and global warming (GW) signal (Fig. 1b, blue dashed curve) both present obvious interdecadal characteristic in the Arctic. Therefore, the global warming signal has limited effect on the interdecadal autumn warming in the Arctic. In addition, the standardized time series of the water vapor and CDLW exhibit consistent variations on both year-to-year variability (dotted curves) and interdecadal variability (solid curves) in Arctic (Fig. 1c). Moreover, their interdecadal turning points from negative anomalies to positive anomalies all occurred in 2001/02 at the 0.01 significance level (Fig. 1d). The average values of t2m with GW (NGW) are -0.79 K (-0.65 K) and 1.1 K (0.89 K) during 1980–2001 and 2002–2017, respectively (Fig. 1b). Next, we will investigate the reason of the Arctic autumn enhanced warming between the two periods (1980–2001 and 2002–2017).

Using the EOF analysis to obtain the main spatiotemporal patterns of the t2m and PW, the leading model (EOF1) for t2m and PW accounted for 56.2% and 36.4% of their total variances, respectively (Fig. 2). According to the EOF1s for t2m and PW, two regions with large variations were located in the Barents-Kara Sea (black box, (0–90°E, 70–84°N))

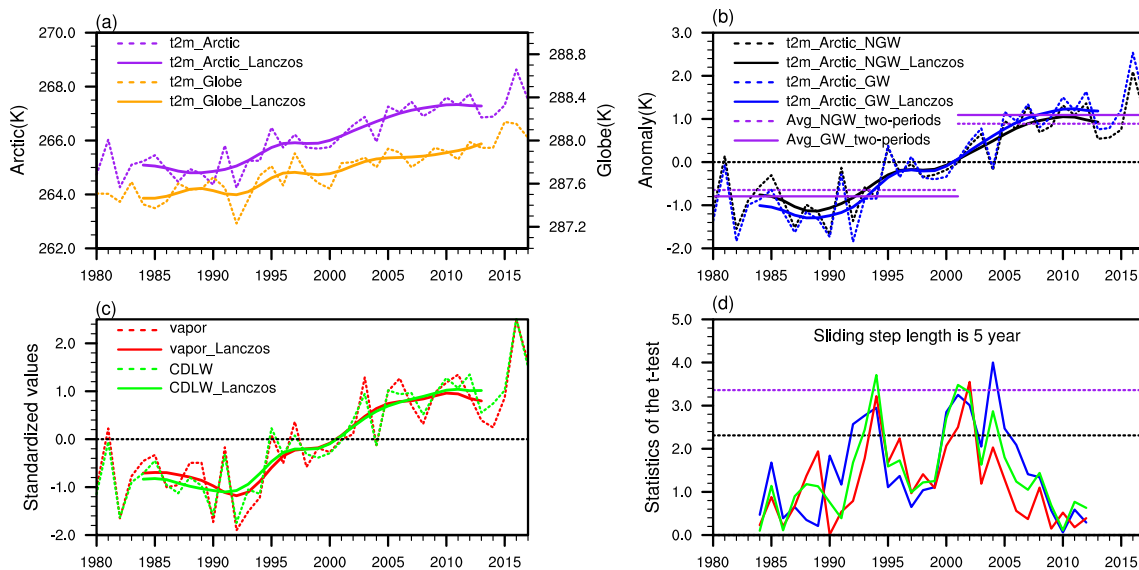


Fig. 1. (a) The autumn year-to-year variability (dashed curves) and interdecadal variability (solid curves, obtained by 9-year Lanczos low-pass filtering) of the 2 m temperature (t2m) in the Arctic (purple curves) and Globe (orange curves). (b) The time series of t2m with global warming (GW, blue curves) and no global warming (NGW, black curves) in autumn (solid curves: interdecadal variability, dashed curves: year-to-year variability), which are the anomaly values. The t2m average values of two periods (1980–2001 and 2002–2017) with GW (purple solid lines) and NGW (purple dashed lines) are also shown. (c) The standardized time series of the water vapor (red curves) and clear-sky downward longwave radiation (CDLW, green curves) in the Arctic in autumn (solid curves: interdecadal variability, dashed curves: year-to-year variability). (d) Sliding t -test of the t2m (blue curve), water vapor (red curve), and CDLW (green curve). The black dashed line represents the 0.05 significance level, and the purple dashed line represents the 0.01 significance level. (For interpretation of the references to colour in this figure legend, the reader is referred to the web version of this article.)

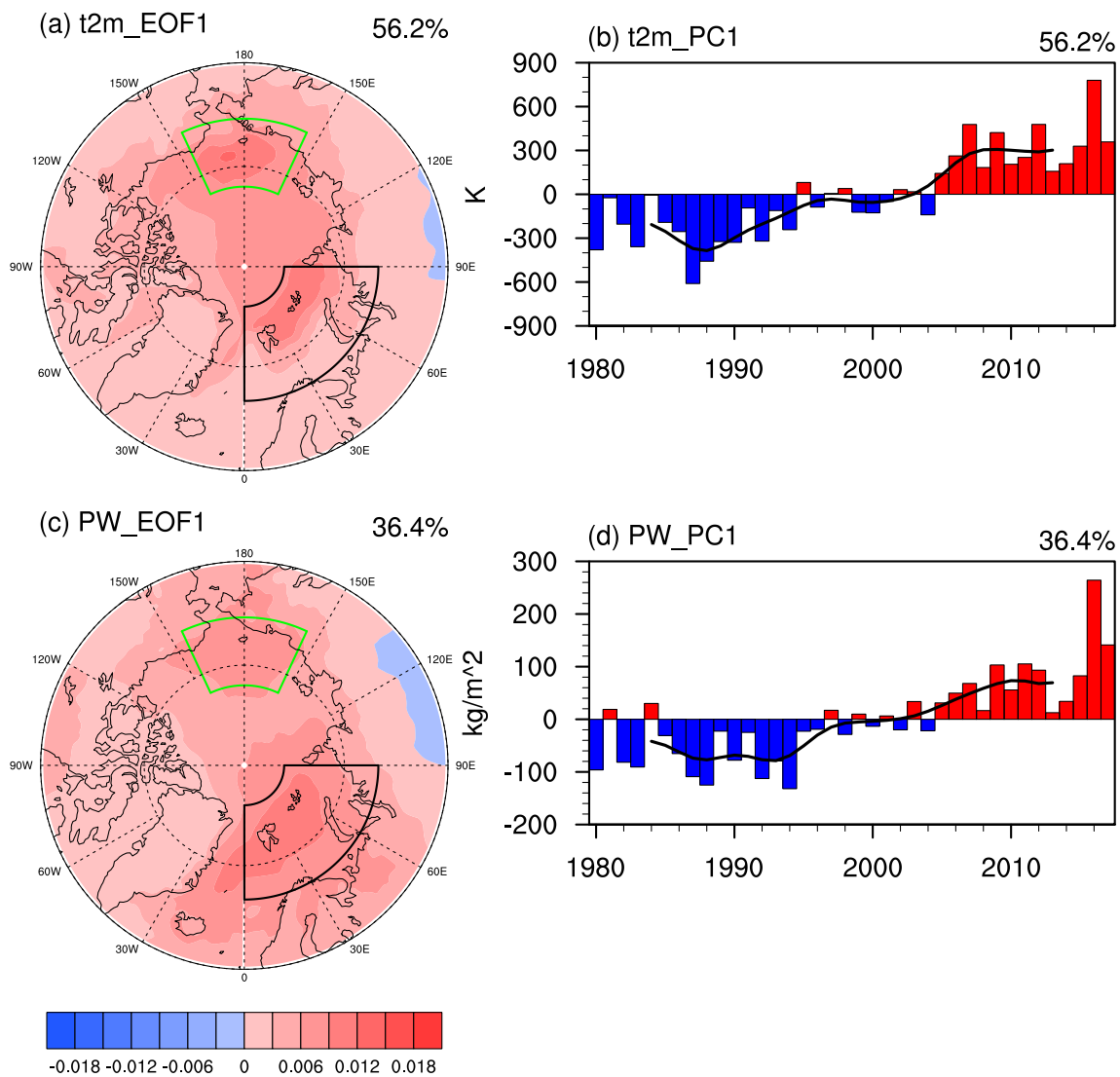


Fig. 2. (a) and (b) The empirical orthogonal function (EOF) analysis for the autumn t2m over the Arctic: (a) the leading model (EOF1), black boxes and green boxes represent the Barents-Kara Sea region ($0\text{--}90^{\circ}\text{E}$, $70\text{--}84^{\circ}\text{N}$) and the Chukchi Sea region ($155\text{--}205^{\circ}\text{E}$, $68\text{--}78^{\circ}\text{N}$), respectively. (b) The first principal component time series (PC1) showing the interdecadal variations (black solid curve; unit: K). (c) and (d) are the same as (a) and (b) but for PW (unit: $\text{kg} \cdot \text{m}^{-2}$).

and the Chukchi Sea (green box, ($155\text{--}205^{\circ}\text{E}$, $68\text{--}78^{\circ}\text{N}$)) (Fig. 2a and c). Moreover, the first principal component (PC1) time series indicates that both the t2m and PW exhibit robust interdecadal variability with interdecadal turning points both occurring in 2001/02 (Fig. 2b and d). These results indicate that the interdecadal spatiotemporal variability in the boreal autumn has been their common and dominant feature in recent decades.

Based on the turning points of the t2m, CDLW, and water vapor, the differences in their spatial distributions between the two periods (2002–2017 minus 1980–2001) are shown in Fig. 3. The increases in the amplitude of the t2m in the northern Barents-Kara Sea and the Chukchi Sea both exceed 3 K (Fig. 3a). In these two regions, the maximum amplitude of the CDLW also exceeded $9 \text{ W} \cdot \text{m}^{-2}$ (Fig. 3b). Moreover, vertically integrated water vapor flux convergence occurs in most area of the Barents-Kara Sea and the Chukchi Sea, which shows that the increase in the water vapor is well correlated with the t2m and CDLW in these two regions (Fig. 3c). As shown for the water vapor flux, the increase in the moisture in the Barents-Kara Sea comes from the North Atlantic, while the water vapor in the Chukchi Sea mainly originates from the North Pacific. Therefore, the interdecadal changes in the t2m, water vapor, and CDLW in the Arctic in autumn exhibit consistent spatiotemporal variations.

3.2. Reasons for water vapor changes in the key regions of the Arctic

Some studies have also shown that the Barents-Kara Sea and the Chukchi Sea are the sensitive regions of climate change in the Arctic. For instance, in winter, atmospheric moisture is transported to the Barents-Kara Sea under certain atmospheric circulation conditions, finally causing significant warming (Luo et al., 2017; Hao et al., 2019; Wang et al., 2020). Not only does the change in the sea ice area in the Chukchi Sea have an important impact on the climate change in Eurasian, but it also regulates the atmospheric circulations by affecting the heat exchange between the ocean and the atmosphere (Ding et al., 2021). Which process plays the leading role in the water vapor convergence in the key regions (i.e., the Barents-Kara Sea and the Chukchi Sea) in autumn? To answer this question, the moisture budget equation was used to determine the causes of the atmospheric water vapor flux convergence.

3.2.1. Relative contributions of the thermodynamics, dynamics, and transient eddy processes to the water vapor changes in the Barents-Kara Sea and the Chukchi Sea

The Barents-Kara Sea, the region in which the atmospheric moisture exhibits convergence, is mainly located in the western sea area of

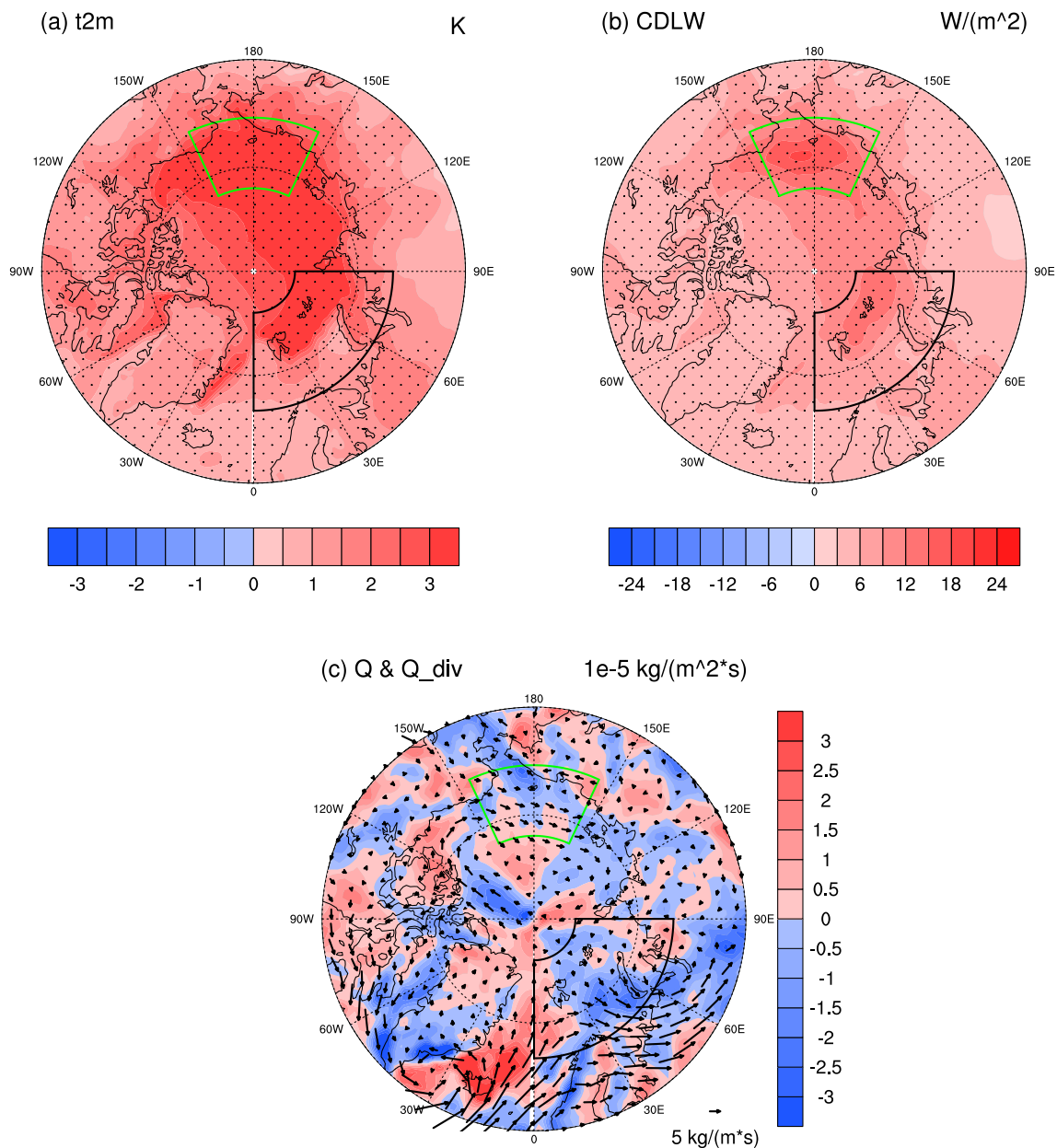


Fig. 3. The autumn difference in the (a) 2 m temperature, (b) clear-sky downward longwave radiation, (c) vertically integrated water vapor flux (vector arrow; unit: $kg \cdot m^{-1} \cdot s^{-1}$), and vertically integrated water vapor flux convergence (shading; unit: $10^{-5} kg \cdot m^{-2} \cdot s^{-1}$) between the two periods (2002–2017 minus 1980–2001) in the Arctic.

Novaya Zemlya, and the maximum value exceeds $2 \times 10^{-5} kg \cdot m^{-2} \cdot s^{-1}$ (Fig. 4a). The result of the moisture budget diagnosis equation shows that the contribution of the change in the mean circulation dynamics (δMCD) plays the dominant role in the atmospheric water vapor convergence compared with the other two processes. This indicates that the interdecadal change in the large-scale atmospheric circulation modulates the change in the water vapor in the Barents-Kara Sea in autumn (Fig. 4c). In addition, the transient eddy (δTE) contributes to the water vapor convergence in western Barents-Kara Sea to a certain extent, indicating that the increase in the water vapor is promoted by the change in the vortex in this region. The contribution of the thermodynamics (δTH) to the water vapor convergence in the eastern and northern parts of the Barents-Kara Sea is much smaller, which reflects the fact that the local water vapor changes have a limited impact on the overall water vapor convergence in the region. Therefore, the moisture in the Barents-Kara Sea mainly comes from outside the region via

transportation by the mean circulations.

In the Chukchi Sea, the divergence of the atmospheric water vapor exhibits divergence in the north and convergence in the south (Fig. 5). The diagnostic results show that the thermodynamics (δTH) make the major contribution to the convergence of the water vapor in the southern-central Chukchi Sea (Fig. 5b), indicating that the local specific humidity exhibits an increase between the two periods. Moreover, the contribution of the dynamics (δMCD) to the atmospheric water vapor convergence mainly occurs in the southeastern Chukchi Sea, which is mainly because the atmospheric circulations promote moisture transport from the North Pacific to the Arctic (Fig. 5c). However, overall, the transient eddy (δTE) restrains the water vapor convergence in the Chukchi Sea (Fig. 5d), indicating that the number of vortices entering the region may decrease between the two periods. Therefore, the δTH and δMCD together promote the increase in water vapor in the Chukchi Sea.

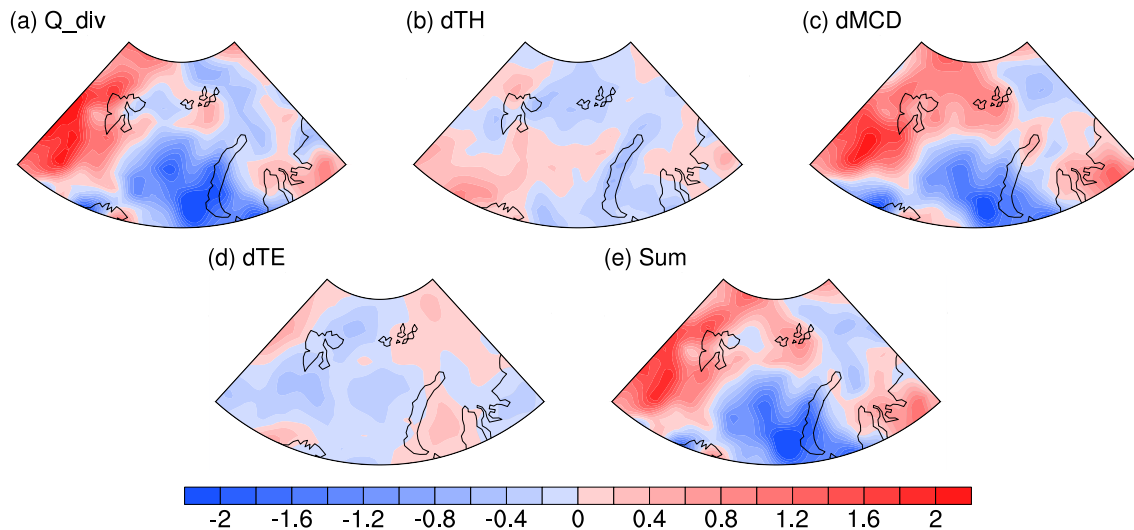


Fig. 4. (a) Changes in the water vapor flux convergence in the Barents-Kara Sea (0–90°E, 70–84°N) in autumn between two periods (2002–2017 minus 1980–2001) (unit: $10^{-5} \text{ kg} \cdot \text{m}^{-2} \cdot \text{s}^{-1}$). The contributions of (b) the thermodynamic component (dTH) via the change in the specific humidity, (c) the dynamic component (dMCD) via the change in the mean circulation, and (d) the transient eddies (dTE) causing the change in water vapor transport. (e) The sum of each contribution (sum).

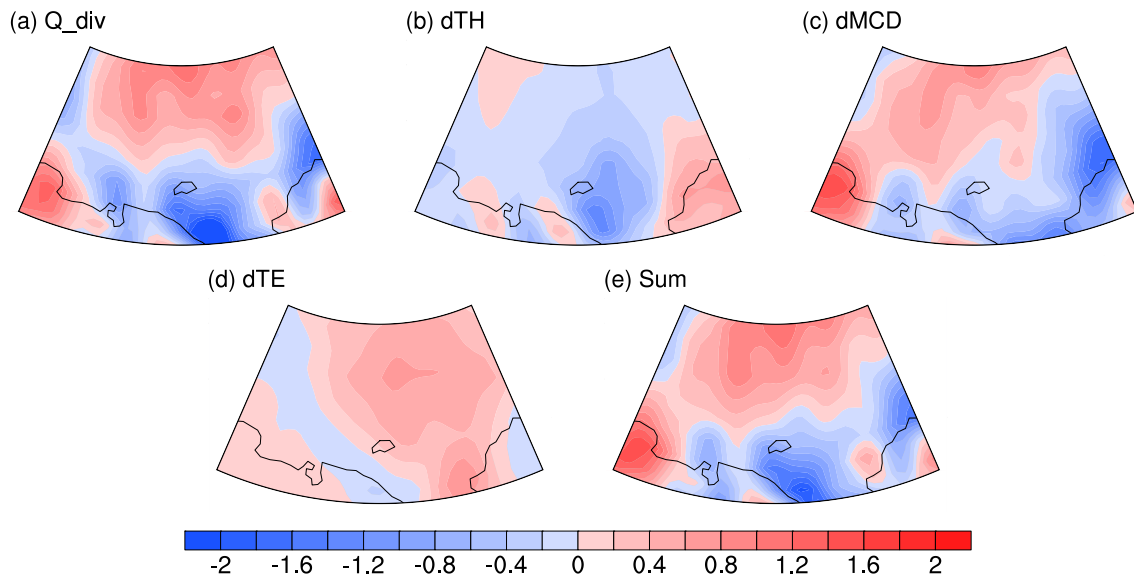


Fig. 5. Same as in Fig. 4, but for the Chukchi Sea (155–205°E, 68–78°N).

3.2.2. Relative contributions of the changes in advection and divergence to the dynamic and thermodynamic components of the water vapor in the Barents-Kara Sea and the Chukchi Sea

In order to explore the effects of moisture advection and divergence on the change in the water vapor, δTH and δMCD were both further divided into the contributions to the changes in the moisture advection (A) and divergence (D) using Eq. (7).

In the Barents-Kara Sea region, the δMCD is the dominate factor that contributes to the convergence of the water vapor flux, which indicates that the difference in the horizontal atmospheric circulation ($[\delta\bar{u}]$), which caused the change in the water vapor flux divergence ($\bar{q}_1 \nabla \cdot [\delta\bar{u}]$), dominates the change in the moisture in autumn (Fig. 6f). In addition, the contribution of the change in the moisture advection dynamics (δMCDA) is smaller because of the smaller gradient in the mean specific humidity ($\nabla \bar{q}_1$) in autumn (Fig. 6e). Although the contribution of δTH is less than that of δMCD , the change in the moisture divergence is also the main reason for the δTH because the variation in the local specific

humidity ($[\delta\bar{q}]$) causes a smaller change in the specific humidity gradient ($\nabla[\delta\bar{q}]$).

In the Chukchi Sea, both δTH (Fig. 7c) and δMCD (Fig. 7g) are dominated by the water vapor divergence (Fig. 7b and f). The increase in the local specific humidity ($\delta\bar{q}$) promotes the overall convergence of the water vapor flux ($-\frac{1}{g} \int_0^{p_s} ([\delta\bar{q}] \nabla \cdot \bar{\mathbf{u}}_1) dp$) in the southern-central Chukchi Sea when the atmospheric circulations is in climatic state (Fig. 7b). However, when the local specific humidity is constant, it is the change in the atmospheric circulation ($\delta\bar{\mathbf{u}}$) that contributes to the overall convergence of the water vapor flux ($-\frac{1}{g} \int_0^{p_s} (\bar{q}_1 \nabla \cdot [\delta\bar{\mathbf{u}}]) dp$). Therefore, the water vapor divergence (D) caused by the changes in the dynamics (δMCDD) and thermodynamics (δTHD) is an important reason for the increase in the water vapor in autumn in the Chukchi Sea.

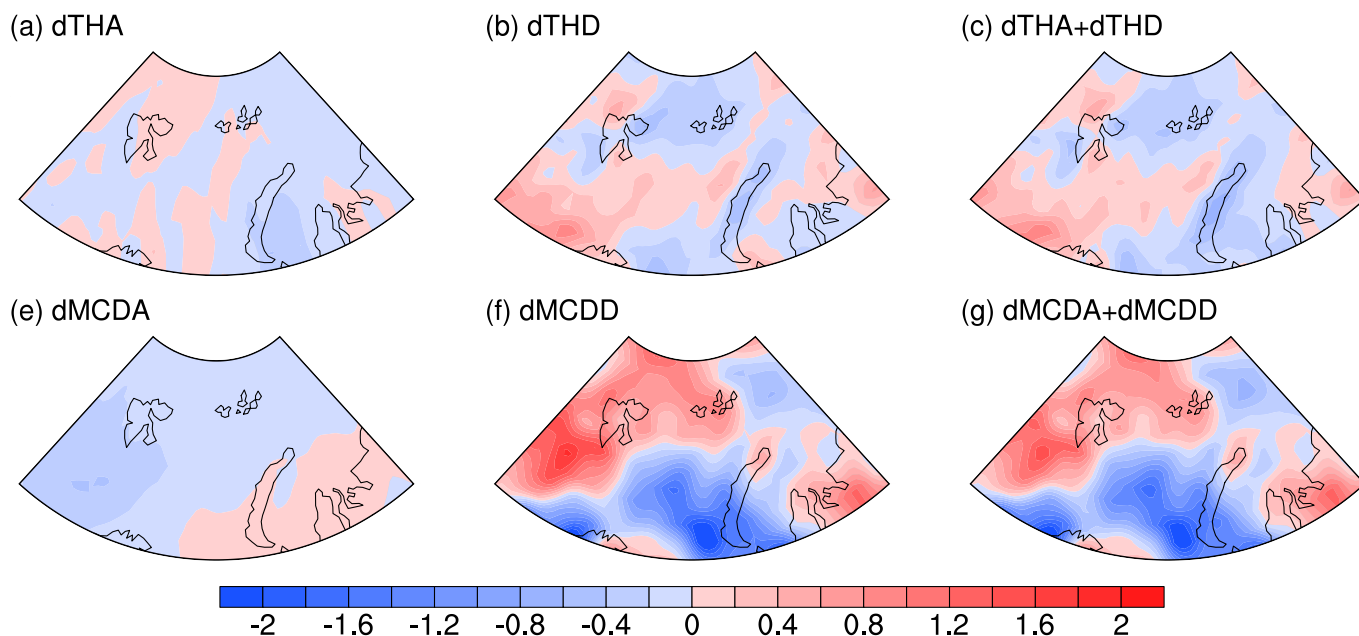


Fig. 6. Differences in the contributions of (a) the moisture advection (dTHA) and (b) moisture divergence (dTHD) to the thermodynamic process (dTH) via the changes in the local humidity and the contributions of the (e) moisture advection (dMCDA) and (f) moisture divergence (dMCDD) to the dynamic processes (dMCD) via changes in the atmospheric circulations (units: $10^{-5} \text{kg} \cdot \text{m}^{-2} \cdot \text{s}^{-1}$) between two time periods (2002–2017 minus 1980–2001) in the Barents-Kara Sea ($0\text{--}90^\circ\text{E}$, $70\text{--}84^\circ\text{N}$) in Autumn. (c) and (g) The sums of the two contributions to the thermodynamic and dynamic processes, respectively.

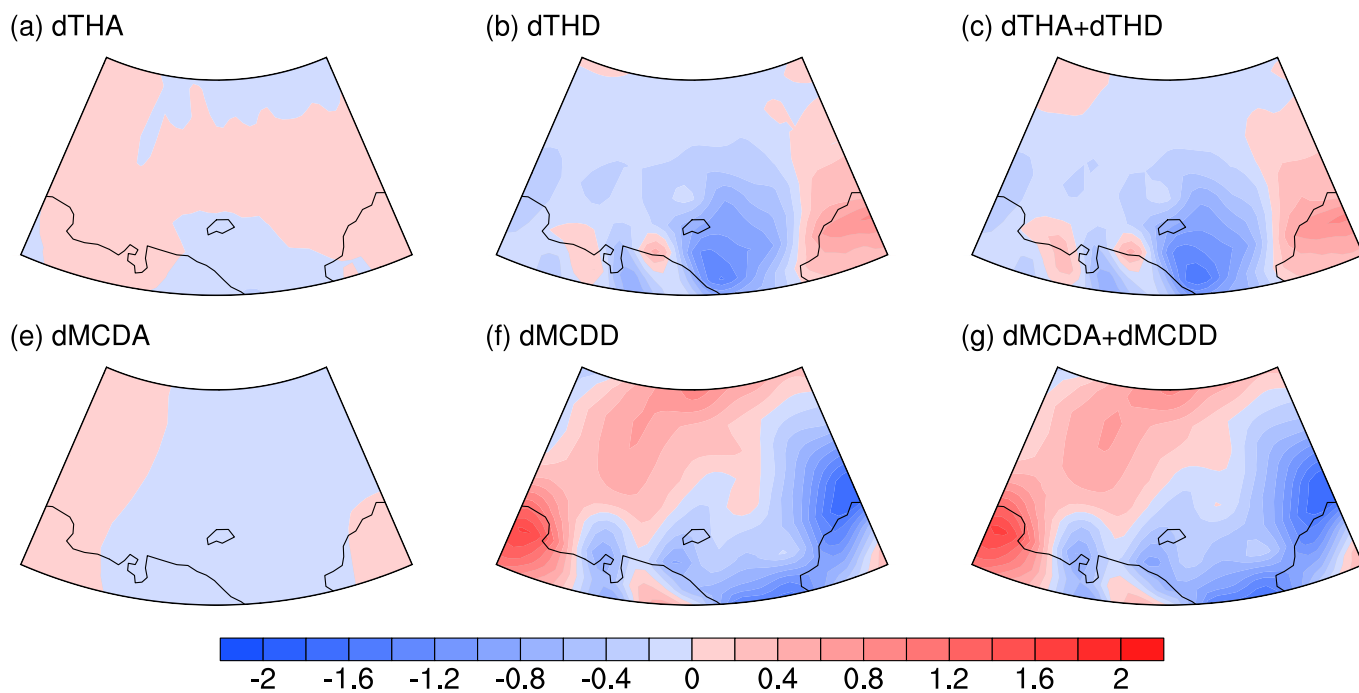


Fig. 7. Same as in Fig. 6, but for the Chukchi Sea ($155\text{--}205^\circ\text{E}$, $68\text{--}78^\circ\text{N}$).

3.3. Contribution of large-scale atmospheric circulations to the change in water vapor

The diagnosis results of the atmospheric water vapor balance equation show that the water vapor convergences over the Barents-Kara Sea and the Chukchi Sea are both influenced by the δMCD in autumn, which is consistent with the results obtained using the Coupled Surface-Atmosphere Climate Feedback Response Analysis Method (CFRAM) (Lu and Cai, 2009; Cai and Lu, 2009). Next, we will further explore which atmospheric circulations affect the increases between the two

periods in the atmospheric water vapor in the two regions.

3.3.1. Role of the AO/NAO in the change in water vapor

Fig. 8 shows the spatiotemporal characteristics of the AO index in JRA-55 dataset. When the AO is in a positive phase, the surface pressure is weaker in the polar region and stronger in mid-latitude region (Fig. 8a). The difference in the PC1 of the AO was positive between 2002–2017 and 1980–2001, which illustrates that the AO index was in the positive phase on the interdecadal scale.

The interdecadal variation in the AO from 1980 to 2017 was used to

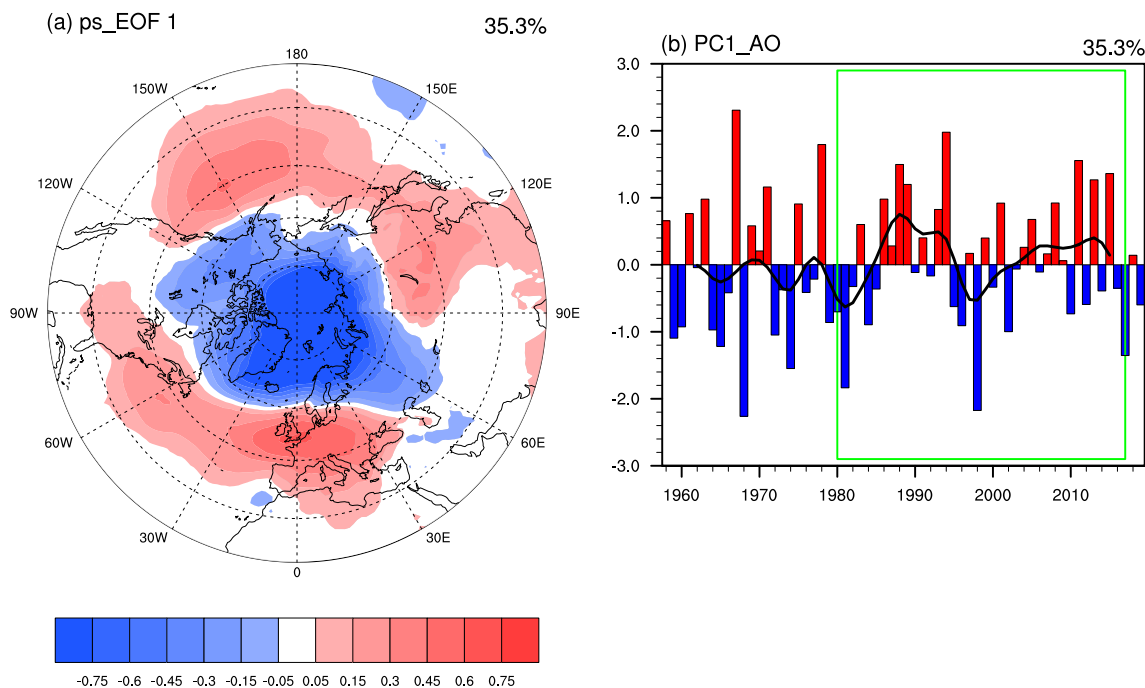


Fig. 8. The spatiotemporal distribution of the Arctic Oscillation (AO) based on the JRA-55 dataset, (a) the leading mode of the surface pressure in the EOF analysis (EOF1), and (b) the first principal component (PC1) time series of the surface pressure in EOF1 (black solid line: the interdecadal change of AO index dealt with low-pass filtering). The period that we focused on is 1980–2017 (the green box). (For interpretation of the references to colour in this figure legend, the reader is referred to the web version of this article.)

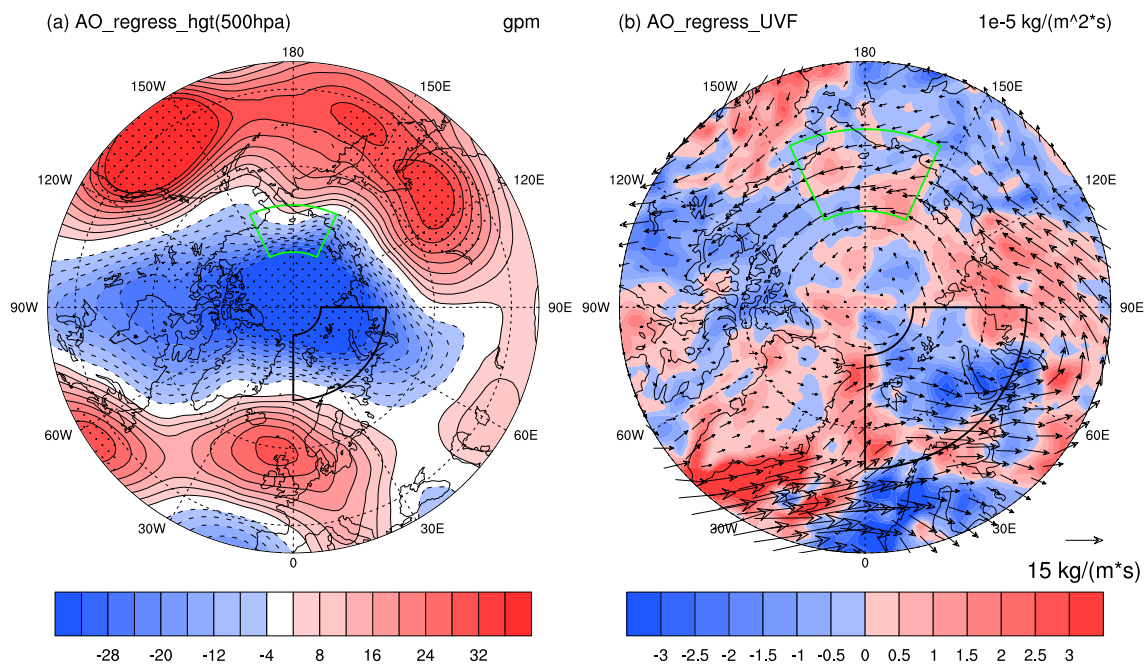


Fig. 9. (a) The interdecadal AO index regresses to the 500 hPa geopotential height (unit: gpm) during 1980–2017. The dotted area represents the 95% significance test. (b) The interdecadal AO index regresses of the vertically integrated water vapor flux (vector, units: $kg \cdot m^{-1} \cdot s^{-1}$) and the atmospheric water vapor flux divergence (shading, units: $10^{-5} kg \cdot m^{-2} \cdot s^{-1}$) during 1980–2017.

regress the geopotential height at 500 hPa, and the results show that the distribution of the geopotential height corresponding to the change in the phase of the AO modulated the moisture transport to the Barents-Kara Sea and the Chukchi Sea where significant accelerated warming was observed in the Arctic. It is obvious that the water vapor was transported from the Northwest Atlantic through the Greenland Sea to the Barents-Kara Sea when the AO was in a positive phase, and the water

vapor convergence mainly occurred in the middle of the Barents-Kara Sea (Fig. 9b). However, the atmospheric circulation related to the positive phase of the AO had a weak impact on the water vapor convergence over the Chukchi Sea (Fig. 9b). For the two regions with significant accelerated warming, the interdecadal positive phase of the AO only contributed to the increase in the autumn water vapor over the Barents-Kara Sea in recent decades.

In some studies, the effects of AO/NAO are considered the same (Cohen and Barlow, 2005; Yadav et al., 2009; Gong et al., 2017b), because NAO is regarded as a part of AO. But other studies found that not only the stratospheric trends of AO and NAO in some seasons were different (Zhou et al., 2001), but also the responses to stratospheric forcing differ between AO and NAO (Rind et al., 2005). A recent study (Hamouda et al., 2021) pointed out that a reduced correlation between NAO and AO indices was detected in most CMIP5 models under global warming. In addition, the NAO reflects the variation in the surface pressure in the North Atlantic and its surrounding regions, while the AO basically reflects the variation in the surface pressure in the entire Northern Hemisphere, except for the tropics. Therefore, a question arises: is the influence of the atmospheric circulation related to the NAO consistent with that related to the AO in the two regions?

To answer this question, the interdecadal variation in the PC1 of the NAO during 1980–2017 was used to regress the geopotential height at 500 hPa (Fig. 11a) and the water vapor (Fig. 11b). The results show that geopotential height exhibits a dipole pattern, with a negative anomaly in the Northern Atlantic sector and a positive anomaly in the Northern Pacific sector. Besides, the difference in the PC1 of the NAO between 2002–2017 and 1980–2001 was also positive (Fig. 10b). The atmospheric circulation associated with the positive phase of the NAO guides the atmospheric water vapor from the North Atlantic through Northern Europe into Siberia and to the Barents-Kara Sea. It also promotes the transport of water vapor from the North Pacific into the Chukchi Sea. When the NAO is in an interdecadal positive phase, it suppresses the water vapor convergence in the Barents-Kara Sea and enhances the water vapor convergence in the southeastern Chukchi Sea, which is different from the effect of the AO. Compared with the thermodynamic effects, the atmospheric dynamics associated with the NAO also cannot be ignored when studying the interdecadal increase in the water vapor in the Chukchi Sea.

3.3.2. Role of the Pacific/North American Pattern in the change in water vapor

Recently, several studies have also reported that the PNA pattern has an important effect on climate change in the Arctic. Zhang et al. (2020) found that the AO, the NAO, and the PNA have more significant influences on Arctic sea-ice loss than the El Niño–Southern Oscillation, the Pacific decadal oscillation (PDO), and the Atlantic multi-decadal oscillation (AMO). In particular, the positive PNA contributes to the Arctic sea-ice loss in the summer. Liu et al. (2021) also stressed that the recent persistent positive PNA pattern has led to increased heat and moisture fluxes from local processes and from advection from the North Pacific

into the western Arctic, which enhanced the lower-tropospheric temperature, humidity, and downward longwave radiation in the western Arctic, finally accelerating the melting of the sea-ice.

On the interdecadal time scale, the difference in the PNA index between 2002–2017 and 1980–2001 is 0.14, which indicates that the variation in the PNA has also been in a positive phase in recent decades (Fig. 12a). Moreover, the water vapor convergence is strengthened in the two regions when the PNA is in the positive phase. In the Barents-Kara Sea, the water vapor convergence mainly occurs in the eastern and central regions, while significant water vapor convergence almost always occurs throughout the Chukchi Sea. It was also found that water vapor is transported from the Northeast Atlantic to the Barents-Kara Sea region when the PNA is in the positive phase, while the water vapor over the Chukchi Sea is mainly transported from the northeastern Pacific.

4. Discussion and conclusions

In this study, we analyzed the spatiotemporal characteristics of the changes in the 2 m temperature (t_{2m}), the precipitable water (PW), and the clear-sky downward longwave radiation (CDLW) over the Arctic in autumn. All of these variables exhibit significant interdecadal increase, with the turning points from negative anomalies to positive anomalies occurring in 2001/02. We further confirmed that the interdecadal variations in the t_{2m} and PW were the dominant characteristics in recent decades, and the significant regions exhibiting increase are mainly located in the Barents-Kara Sea and the Chukchi Sea in autumn. Moreover, the difference in the atmospheric water vapor flux shows that the water vapor over the Barents-Kara Sea is mainly transported from the Northern Atlantic, while the water vapor over the Chukchi Sea is transported from the Northern Pacific Ocean.

To further reveal the reason for the increase in the water vapor in the Barents-Kara Sea and the Chukchi Sea, the atmospheric moisture budget diagnosis equation was used. The diagnosis results show that the moisture convergence in the Barents-Kara Sea is mainly affected by the water vapor divergence caused by the changes in the mean circulation dynamics (δMCD), while both the δMCD and the changes in the local specific humidity thermodynamics (δTH) contribute to the moisture convergence in the Chukchi Sea. The transient eddy (δTE) has a limited impact on the change in the water vapor divergence in these two regions.

By analyzing the changes in the atmospheric circulations associated with the AO, NAO, and PNA in recent decades, it is found that the positive phase of AO plays the dominant role in the increase in the water vapor in the Barents-Kara Sea, but it has a limited effect on the change in

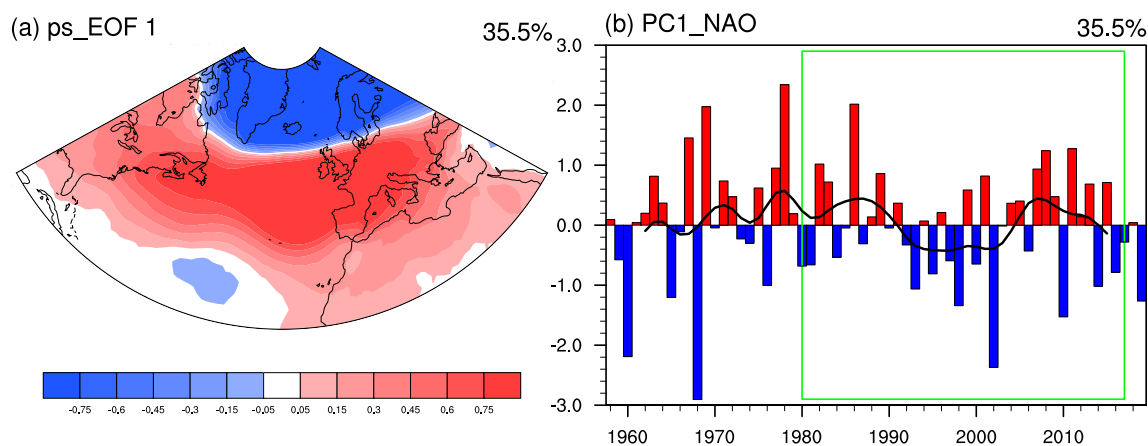


Fig. 10. The spatiotemporal distribution of the North Atlantic Oscillation (NAO) based on the JRA-55 dataset. (a) The leading mode of the surface pressure in the EOF analysis (EOF1), and (b) the first principal component (PC1) of the surface pressure in EOF1 (black solid line: the interdecadal change in the NAO index dealt with low-pass filtering). The time period that we focused on was 1980–2017 (green box). (For interpretation of the references to colour in this figure legend, the reader is referred to the web version of this article.)

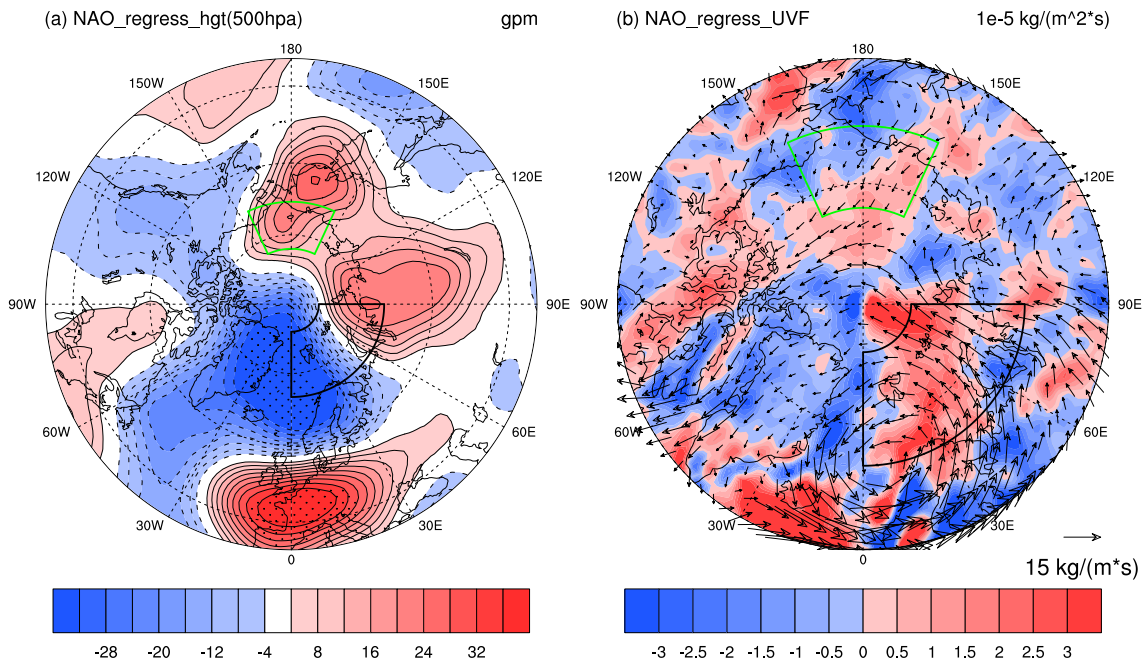


Fig. 11. (a) The interdecadal NAO index regresses to the 500 hPa geopotential height (units: gpm) during 1980–2017. The dotted area represents the 95% significance test. (b) The interdecadal NAO index regresses to the vertically integrated water vapor flux (vector, units: $kg \cdot m^{-1} \cdot s^{-1}$) and the atmospheric water vapor flux divergence (shading, units: $10^{-5} kg \cdot m^{-2} \cdot s^{-1}$) during 1980–2017.

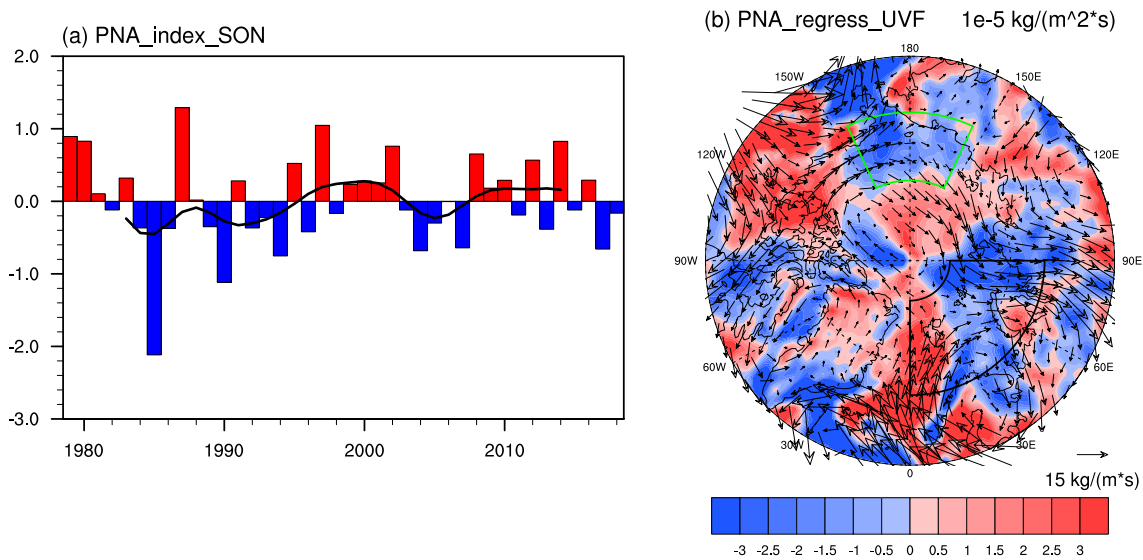


Fig. 12. (a) Variation in the PNA index during 1979–2018 (black solid line: the interdecadal variation dealt with low-pass filtering). (b) The interdecadal PNA index regresses to the vertically integrated water vapor flux (vector, units: $kg \cdot m^{-1} \cdot s^{-1}$) and the atmospheric water vapor flux divergence (shading, units: $10^{-5} kg \cdot m^{-2} \cdot s^{-1}$) during 1980–2017.

the water vapor in the Chukchi Sea. However, the positive phase of NAO promotes the increase in the water vapor in the Chukchi Sea but suppresses the water vapor convergence in the Barents-Kara Sea. For the positive phase of PNA, the associated atmospheric circulation contributes to the water vapor convergence in both regions. The results also show that the effects of the different atmospheric circulations on the regional climate change in the Arctic are different. A schematic diagram of the results of this study is provided in Fig. 13.

Numerous previous studies mainly have focused on the response of atmospheric circulations (NAO/AO, Ural blocking) to the warming and/or sea ice loss in the Arctic (Screen et al., 2013; Yang et al., 2016; Yao et al., 2017; Luo et al., 2017; Simon et al., 2020; Chen et al., 2021). In the

study, we emphasized the contribution of the atmospheric water vapor transported by the horizontal atmospheric circulations to the Arctic warming in autumn. Besides, Lei et al. (2019) found that the atmospheric circulation had an impact on the drift trajectories of sea ice in Arctic Ocean. Some studies also stressed that the atmospheric circulations associated with Greenland High or Ural blocking contributed to the Arctic warming in Winter (Luo et al., 2018; Champagne et al., 2019). Therefore, the contribution of the large-scale atmospheric circulation to the Arctic warming cannot be ignored.

In this study, we emphasized the key role of large-scale circulations induced internal variability in the Arctic autumn warming. Although the large-scale circulations, such as AO/NAO/PNA, have their own temporal

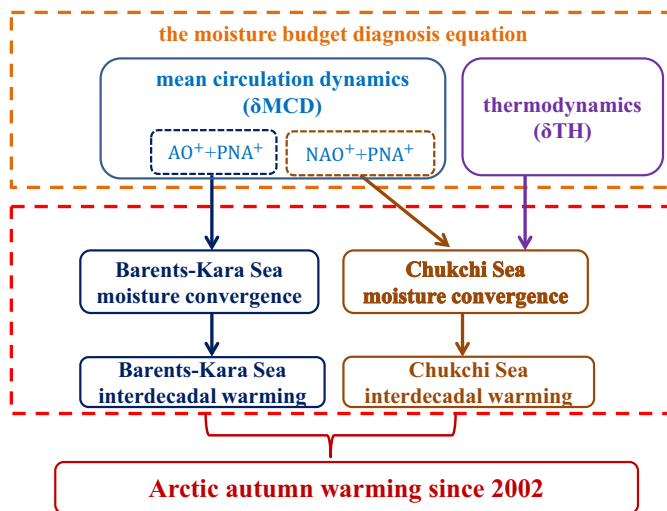


Fig. 13. Schematic diagram shows the mechanism modulating the Arctic autumn warming since 2002.

features in phase and magnitude, their combined effects on regional climate may result in a decadal change in t2m/moisture between 1980–2001 and 2002–2017. Besides, the Arctic autumn warming may also be affected by some other factors, such as the external forcing. This is one of the reasons why the interdecadal changes of AO/NAO/PNA are not completely consistent with the interdecadal change in t2m. Therefore, the contribution of the sea-ice albedo feedback was limited compared with other processes (Gao et al., 2019), but some studies have also investigated the other roles of sea-ice (external forcing) in autumn warming. For instance, Wu and Lee (2012) found that the decrease in the Arctic sea-ice extent has led to more evaporation over the open water in summer and a subsequent increase in the low clouds, which has enhanced the autumnal warming in the Arctic. Cao et al. (2019) stressed that the reduction of Arctic sea-ice has enhanced the sea-ice-air interactions in the Arctic atmospheric boundary layer, especially the increase in the sea-air heat flux in autumn. Through numerical experiments, Suo et al. (2016) found that the disappearance of the autumn Arctic sea-ice can cause significant synchronous near-surface warming over regions where sea-ice is removed.

In future studies, the mechanisms of the dominant factors causing the Arctic warming could be explored based on this diagnosis, which can be beneficial to resolving the debate as to the importance of the different factors to the Arctic warming.

Declaration of Competing Interest

The authors declare that they have no known competing financial interests or personal relationships that could have appeared to influence the work reported in this paper.

Acknowledgement

This work was supported by the Strategic Priority Research Program of the Chinese Academy of Sciences (grant numbers XDA19070404 and XDA20060401), the National Natural Science Foundation of China (grant numbers 41725018 and 91637312) and the National Key Research and Development Program of China (grant number 2018YFC1505604). We also thank the reviewers for their valuable suggestions for our manuscript.

References

Adrian, J.S., Paul, P., 2015. Arctic warming in ERA-Interim and other analyses. *Quart. J. R. Meteor. Soc.* 141, 1147–1162. <https://doi.org/10.1002/qj.2422>.

- Beer, E., Eisenman, I., Wagner, T., 2020. Polar amplification due to enhanced heat flux across the halocline. *Geophys. Res. Lett.* 47, e2019GL086706 <https://doi.org/10.1029/2019GL086706>.
- Boisvert, L.N., Stroeve, J.C., 2015. The Arctic is becoming warmer and wetter as revealed by the Atmospheric Infrared Sounder. *Geophys. Res. Lett.* 42, 4439–4446. <https://doi.org/10.1002/2015GL063775>.
- Bony, S., Colman, R., Kattsov, V., et al., 2006. How well do we understand and evaluate climate change feedback processes? *J. Clim.* 19, 3445–3482. <https://doi.org/10.1175/JCLI3819.1>.
- Cai, M., Lu, J.H., 2009. A new framework for isolating individual feedback processes in coupled general circulation climate models. Part II: method demonstrations and comparisons. *Clim. Dyn.* 32, 887–900. <https://doi.org/10.1007/s00382-008-0425-3>.
- Cai, Z., You, Q., Wu, F., Chen, H.W., Chen, D., Cohen, J., 2021. Arctic warming revealed by multiple CMIP6 models: evaluation of historical simulations and quantification of future projection uncertainties. *J. Clim.* 34, 4871–4892. <https://doi.org/10.1175/JCLI-D-20-0791.1>.
- Cao, Y., Bian, L.G., Zhao, J.P., 2019. Impacts of changes in Sea Ice and Heat Flux on Arctic Warming. *Atmos. Clim. Sci.* 9, 84–99. <https://doi.org/10.4236/acs.2019.91006>.
- Champagne, O., Pohl, B., McKenzie, S., et al., 2019. Atmospheric circulation modulates the spatial variability of temperature in the Atlantic–Arctic region. *Int. J. Climatol.* 39, 3619–3638. <https://doi.org/10.1002/joc.6044>.
- Chen, H.W., Zhang, Q., Körnich, H., Chen, D., 2013. A robust mode of climate variability in the Arctic: the Barents Oscillation. *Geophys. Res. Lett.* 40, 2856–2861. <https://doi.org/10.1002/grl.5055>.
- Chen, X., Luo, D., Wu, Y., Dunn-Sigouin, E., Lu, J., 2021. Nonlinear response of atmospheric blocking to early winter Barents–Kara Seas warming: an Idealized Model Study. *J. Clim.* 34, 2367–2383. <https://doi.org/10.1175/JCLI-D-19-0720.1>.
- Clark, J., Shenoy, V., Feldstein, S., Lee, S., Goss, M., 2021. The role of horizontal temperature advection on Arctic amplification. *J. Clim.* 34, 2957–2976. <https://doi.org/10.1175/JCLI-D-19-0937.1>.
- Cohen, J., Barlow, M., 2005. The NAO, the AO, and Global Warming: how closely related? *J. Clim.* 18, 4498–4513. <https://doi.org/10.1175/JCLI3530.1>.
- Coumou, D., Di Capua, G., Vavrus, S., et al., 2018. The influence of Arctic amplification on mid-latitude summer circulation. *Nat. Commun.* 9, 2959. <https://doi.org/10.1038/s41467-018-05256-8>.
- Crook, J., Forster, P., Stuber, N., 2011. Spatial patterns of modeled climate feedback and contributions to temperature response and polar amplification. *J. Clim.* 24, 3575–3592. <https://doi.org/10.1175/2011JCLI3863.1>.
- Curry, J.A., Schramm, J.L., Serreze, M.C., Ebert, E.E., 1995. Water vapor feedback over the Arctic Ocean. *J. Geophys. Res.* 100, 14223–14229. <https://doi.org/10.1029/95JD00824>.
- Dai, A., Luo, D., Song, M., et al., 2019. Arctic amplification is caused by sea-ice loss under increasing CO₂. *Nat. Commun.* 10, 121. <https://doi.org/10.1038/s41467-018-07954-9>.
- Ding, S., Wang, B., Chen, W., 2021. Dominant characteristics of early autumn Arctic sea ice variability and its impact on winter Eurasian climate. *J. Clim.* 34, 1825–1846. <https://doi.org/10.1175/JCLI-D-19-0834.1>.
- Duchon, C., 1979. Lanczos filtering in one and two dimensions. *J. Appl. Meteorol.* 18, 1016–1022. [https://doi.org/10.1175/1520-0450\(1979\)018<1016:LFIQAT>2.0.CO;2](https://doi.org/10.1175/1520-0450(1979)018<1016:LFIQAT>2.0.CO;2).
- Ebita, A., Kobayashi, S., Ota, Y., et al., 2011. The Japanese 55-year reanalysis “JRA-55”: an interim report. *SOLA 7*, 149–152. <https://doi.org/10.2151/sola.2011-038>.
- Gao, Y., Cuo, L., Zhang, Y., 2014. Changes in moisture flux over the Tibetan Plateau during 1979–2011 and possible mechanisms. *J. Clim.* 27, 1876–1893. <https://doi.org/10.1175/JCLI-D-13-00321.1>.
- Gao, K., Duan, A., Chen, D., Wu, G., 2019. Surface energy budget diagnosis reveals possible mechanism for the different warming rate among Earth's three poles in recent decades. *Sci. Bull.* 64, 1140–1143. <https://doi.org/10.1016/j.scib.2019.06.023>.
- Ghatak, D., Miller, J., 2013. Implications for Arctic amplification of changes in the strength of the water vapor feedback. *J. Geophys. Res.-Atmos.* 118, 7569–7578. <https://doi.org/10.1002/jgrd.50578>.
- Gong, T., Feldstein, S., Lee, S., 2017a. The role of downward infrared radiation in the recent Arctic winter warming trend. *J. Clim.* 30, 4937–4949. <https://doi.org/10.1175/JCLI-D-16-0180.1>.
- Gong, D.Y., Guo, D., Li, S., Kim, S.J., 2017b. Winter AO/NAO modifies summer ocean heat content and monsoonal circulation over the western Indian Ocean. *J. Meteorol. Res.* 31, 94–106. <https://doi.org/10.1007/s13351-017-6175-6>.
- Goosse, H., Kay, J.E., Armour, K.C., et al., 2018. Quantifying climate feedbacks in polar regions. *Nat. Commun.* 9, 1919. <https://doi.org/10.1038/s41467-018-04173-0>.
- Gordon, N.D., Jonko, A.K., Forster, P.M., Shell, K.M., 2013. An observationally based constraint on the water–vapor feedback. *J. Geophys. Res.-Atmos.* 118, 1–9. <https://doi.org/10.1002/2013JD020184>.
- Graversen, R., Burtu, M., 2016. Arctic amplification enhanced by latent energy transport of atmospheric planetary waves. *Quart. J. R. Meteor. Soc.* 142, 2046–2054. <https://doi.org/10.1002/qj.2802>.
- Graversen, R., Wang, M., 2009. Polar amplification in a coupled climate model with locked albedo. *Clim. Dyn.* 33, 629–643. <https://doi.org/10.1007/s00382-009-0535-6>.
- Hamouda, M.E., Pasquero, C., Tziperman, E., 2021. Decoupling of the Arctic Oscillation and North Atlantic Oscillation in a warmer climate. *Nat. Clim. Chang.* 11, 137–142. <https://doi.org/10.1038/s41558-020-00966-8>.
- Hao, M., Luo, Y., Lin, Y., Zhao, Z., Wang, L., Huang, J., 2019. Contribution of atmospheric moisture transport to winter Arctic warming. *Int. J. Climatol.* 39, 2697–2710. <https://doi.org/10.1002/joc.5982>.

- Hegyí, B., Taylor, P., 2017. The regional influence of the Arctic Oscillation and Arctic Dipole on the wintertime Arctic surface radiation budget and sea ice growth. *Geophys. Res. Lett.* 44, 4341–4350. <https://doi.org/10.1002/2017GL073281>.
- Jeong, J.-H., Kug, J.-S., Linderholm, H.W., Chen, D., Kim, B.-M., Jun, S.-Y., 2014. Intensified Arctic warming under greenhouse warming by vegetation-atmosphere-sea ice interaction. *Environ. Res. Lett.* 9, 094007 <https://doi.org/10.1088/1748-9326/9/9/094007>.
- Kobayashi, S., Ota, Y., Harada, Y., Ebita, A., Moriya, M., Onoda, H., Onogi, K., Kamahori, H., Kobayashi, C., Endo, H., Miyaoka, K., Takahashi, K., 2015. The JRA-55 reanalysis: general specifications and basic characteristics. *J. Meteor. Soc. Japan* 93, 5–48. <https://doi.org/10.2151/jmsj.2015-001>.
- Lei, R., Gui, D., Hutchings, J.K., Wang, J., Pang, X., 2019. Backward and forward drift trajectories of sea ice in the northwestern Arctic Ocean in response to changing atmospheric circulation. *Int. J. Climatol.* 39, 4372–4391. <https://doi.org/10.1002/joc.6080>.
- Liu, Z., Risi, C., Codron, F., et al., 2021. Acceleration of western Arctic sea ice loss linked to the Pacific North American pattern. *Nat. Commun.* 12, 1519. <https://doi.org/10.1038/s41467-021-21830-z>.
- Lu, J., Cai, M., 2009. A new framework for isolating individual feedback processes in coupled general circulation climate models. Part I: Formulation. *Clim. Dyn.* 32, 873–885. <https://doi.org/10.1007/s00382-008-0425-3>.
- Luo, B., Luo, D., Wu, L., Zhong, L., Simmonds, I., 2017. Atmospheric circulation patterns which promote winter Arctic sea ice decline. *Environ. Res. Lett.* 12, 054017 <https://doi.org/10.1088/1748-9326/aa69d0>.
- Luo, D.H., Chen, X.D., Dai, A.G., Simmonds, I., 2018. Changes in atmospheric blocking circulations linked with winter Arctic warming: a new perspective. *J. Clim.* 31, 7661–7678. <https://doi.org/10.1175/JCLI-D-18-0040.1>.
- Middlemas, E., Kay, J., Medeiros, B., Maroon, E., 2020. Quantifying the influence of cloud radiative feedbacks on Arctic surface warming using cloud locking in an Earth system model. *Geophys. Res. Lett.* 47, e2020GL089207 <https://doi.org/10.1029/2020GL089207>.
- National Center for Atmospheric Research Staff (NCAR), 2021. The Climate Data Guide: Hurrell North Atlantic Oscillation (NAO) Index (PC-based). Retrieved from <https://climatedataguide.ucar.edu/climate-data/hurrell-north-atlantic-oscillation-nao-index-pc-based>.
- Pithan, F., Mauritsen, T., 2014. Arctic amplification dominated by temperature feedbacks in contemporary climate models. *Nat. Geosci.* 7, 181–184. <https://doi.org/10.1038/ngeo2071>.
- Previdi, M., Janoski, T., Chiodo, G., Smith, K., Polvani, L., 2020. Arctic amplification: a rapid response to radiative forcing. *Geophys. Res. Lett.* 47, e2020GL089933 <https://doi.org/10.1029/2020GL089933>.
- Rind, D., Perlwitz, J., Lonergan, P., 2005. AO/NAO response to climate change: 1. Respective influences of stratospheric and tropospheric climate changes. *J. Geophys. Res.* 110, D12107 <https://doi.org/10.1029/2004JD005103>.
- Rinke, A., Segger, B., Crewell, S., et al., 2019. Trends of vertically integrated water vapor over the Arctic during 1979–2016: consistent moistening all over? *J. Clim.* 32, 6079–6116. <https://doi.org/10.1175/JCLI-D-19-0092.1>.
- Screen, J., Simmonds, I., 2010. The central role of diminishing sea ice in recent Arctic temperature amplification. *Nature* 464, 1334–1337. <https://doi.org/10.1038/nature09051>.
- Screen, J., Simmonds, I., Deser, C., Tomas, R., 2013. The atmospheric response to three decades of observed Arctic sea ice loss. *J. Clim.* 26, 1230–1248. <https://doi.org/10.1175/JCLI-D-12-00063.1>.
- Seager, R., Vecchi, G., 2010. Greenhouse warming and the 21st century hydroclimate of southwestern North America. *Proc. Natl. Acad. Sci. U. S. A.* 107 (21), 277–21282. <https://doi.org/10.1073/pnas.0910856107>.
- Seager, R., Ting, M., Held, I., Kushnir, Y., Lu, J., Vecchi, G., Huang, H.-P., Harnik, N., Leetmaa, A., Lau, N.-C., Li, C., Velez, J., Naik, N., 2007. Model projections of an imminent transition to a more arid climate in Southwestern North America. *Science* 316, 1181–1184. <https://doi.org/10.1126/science.1139601>.
- Seager, R., Naik, N., Vecchi, G., 2010. Thermodynamic and dynamic mechanisms for large-scale changes in the hydrological cycle in response to global warming. *J. Clim.* 23, 4651–4668. <https://doi.org/10.1175/2010JCLI3655.1>.
- Serreze, M.C., Francis, J.A., 2006. The Arctic amplification debate. *Clim. Chang.* 2006 (76), 241–264. <https://doi.org/10.1007/s10584-005-9017-y>.
- Serreze, M.C., Walsh, J.E., Chapin, F.S., et al., 2000. Observational evidence of recent change in the Northern high-latitude environment. *Clim. Chang.* 46, 159–207. <https://doi.org/10.1023/A:1005504031923>.
- Shupe, M., Intrieri, J., 2004. Cloud radiative forcing of the Arctic surface: the influence of cloud properties, surface albedo, and solar zenith angle. *J. Clim.* 17, 616–628. [https://doi.org/10.1175/1520-0442\(2004\)017<0616:CRFOTA>2.0.CO;2](https://doi.org/10.1175/1520-0442(2004)017<0616:CRFOTA>2.0.CO;2).
- Simon, A., Frankignoul, C., Gastineau, G., Kwon, Y., 2020. An observational estimate of the direct response of the cold-season atmospheric circulation to the Arctic sea ice loss. *J. Clim.* 33, 3863–3882. <https://doi.org/10.1175/JCLI-D-19-0687.1>.
- Stuecker, M.F., Bitz, C.M., Armour, K.C., et al., 2018. Polar amplification dominated by local forcing and feedbacks. *Nat. Clim. Chang.* 8, 1076–1081. <https://doi.org/10.1038/s41558-018-0339-y>.
- Suo, L., Gao, Y., Guo, D., Liu, J., Wang, H., Johannessen, O., 2016. Atmospheric response to the autumn sea-ice free Arctic and its detectability. *Clim. Dyn.* 46, 2051–2066. <https://doi.org/10.1007/s00382-015-2689-8>.
- Taylor, P., Cai, M., Hu, A., et al., 2013. A decomposition of feedback contributions to polar warming amplification. *J. Clim.* 26, 7023–7043. <https://doi.org/10.1175/JCLI-D-12-00696.1>.
- Trenberth, K., Guillemot, C.J., 1995. Evaluation of the global atmospheric moisture budget as seen from analyses. *J. Clim.* 8, 2255–2272. [https://doi.org/10.1175/1520-0442\(1995\)008<2255:EOTGAM>2.0.CO;2](https://doi.org/10.1175/1520-0442(1995)008<2255:EOTGAM>2.0.CO;2).
- Wallace, J., Gutzler, D., 1981. Teleconnections in the geopotential height field during the Northern Hemisphere winter. *Mon. Weather Rev.* 109, 784–812. [https://doi.org/10.1175/1520-0493\(1981\)109<0784:TITGHF>2.0.CO;2](https://doi.org/10.1175/1520-0493(1981)109<0784:TITGHF>2.0.CO;2).
- Wang, S., Chen, W., Chen, S., Nath, D., Wang, L., 2020. Anomalous winter moisture transport associated with the recent surface warming over the Barents–Kara seas region since the mid-2000s. *Int. J. Climatol.* 40, 2497–2505. <https://doi.org/10.1002/joc.6337>.
- Weare, B.C., Nasstrom, J.S., 1982. Examples of extended empirical orthogonal function analyses. *Mon. Weather Rev.* 110, 481–485. [https://doi.org/10.1175/1520-0493\(1982\)110<0481:EOEEOF>2.0.CO;2](https://doi.org/10.1175/1520-0493(1982)110<0481:EOEEOF>2.0.CO;2).
- Weare, B.C., Newell, R.E., 1977. Empirical orthogonal analysis of Atlantic Ocean surface temperatures. *Quart. J. R. Meteor. Soc.* 103, 467–478. <https://doi.org/10.1002/qj.49710343707>.
- Wu, D.L., Lee, J.N., 2012. Arctic low cloud changes as observed by MISR and CALIOP: Implication for the enhanced autumnal warming and sea ice loss. *J. Geophys. Res.* 117, D07107 <https://doi.org/10.1029/2011JD017050>.
- Yadav, R.K., Rupa Kumar, K., Rajeevan, M., 2009. Increasing influence of ENSO and decreasing influence of AO/NAO in the recent decades over Northwest India winter precipitation. *J. Geophys. Res.* 114, D12112 <https://doi.org/10.1029/2008JD011318>. doi:10.1029/2008JD011318.
- Yang, X., Yuan, X., Ting, M., 2016. Dynamical link between the Barents–Kara sea ice and the Arctic oscillation. *J. Clim.* 29, 5103–5122. <https://doi.org/10.1175/JCLI-D-15-0669.1>.
- Yao, Y., Luo, D., Dai, A., Simmonds, I., 2017. Increased quasi stationarity and persistence of winter ural blocking and Eurasian extreme cold events in response to Arctic warming. Part I: Insights from Observational Analyses. *J. Clim.* 30, 3549–3568. <https://doi.org/10.1175/JCLI-D-16-0261.1>.
- You, Q., Cai, Z., Pepin, N., Chen, D., Ahrens, B., Jiang, Z., Wu, F., Kang, S., Zhang, R., Wu, T., Wang, P., Li, M., Zuo, Z., Gao, Y., Zhai, P., Zhang, Y., 2021. Warming amplification over the Arctic Pole and Third Pole: Trends, mechanisms and consequences. *Earth-Sci. Rev.* 217, 103625. <https://doi.org/10.1016/j.earscirev.2021.103625>.
- Zhang, S., Gant, T.Y., Bush, A.B.G., 2020. Variability of Arctic sea ice based on quantile regression and the teleconnection with large-scale climate patterns. *J. Clim.* 33, 4009–4025. <https://doi.org/10.1175/JCLI-D-19-0375.1>.
- Zhou, S., Miller, A.J., Wang, J., Angell, J.K., 2001. Trends of NAO and AO and their associations with stratospheric processes. *Geophys. Res. Lett.* 28, 4107–4110. <https://doi.org/10.1029/2001GL013660>.